



Electrochemical and structural study of LiCoPO_4 -based Electrodes

Dr. Ravindra Singh Yadav

Associate Professor

Department Of Chemistry M.M.H. College Ghaziabad (U.P.) India.

Abstract:

LiCoPO_4 samples were synthesized by two different techniques (high-temperature solid-state reaction and lower-temperature synthesis using $\text{NH}_4\text{Co-PO}_4\cdot\text{H}_2\text{O}$ as precursor) and tested as cathode materials for 5-V lithium batteries. An irreversible lithium deinsertion was observed for the high-temperature sample. In contrast, the application of lower-temperature synthesis led to a significant improvement of the lithium storage reversibility. Different delithiation mechanisms in LiCoPO_4 were found for the samples obtained by different synthetic techniques. The nature of capacity fading during cycling of the cells is discussed.

Keywords: Rechargeable batteries, Intercalation, Lithium, Olivine-type structure, Cathode.

1. Introduction:

During recent years, many studies on lithium recharge-able batteries have been carried out to develop new materials with high specific energy. For a long time, the layered lithium-cobalt and cobalt-nickel oxides, operate in the 4-V region, as well as lithium manganese oxide with the spinel structure, have been recognized as promising cathode materials [1, 2, 3, 4]. In the future, real alternatives leading to higher energy densities of power sources could be materials intercalating lithium ions in a reversible manner at high potential vs. metallic lithium. Furthermore, these materials can be combined with a variety of negative electrodes other than metallic lithium or carbon and still operate at high cell voltages.

Operation at high potentials is associated with some difficulties caused by the instability of the commonly used nonaqueous lithium electrolytes at potentials above 4 V, and by the possible corrosion of components of the electrochemical cell. Nevertheless, the materials intercalating Li ions at potentials close to 5 V versus metallic Li, such as substituted spinels $\text{LiM}_x\text{Mn}_{2-x}\text{O}_4$ ($\text{M}=\text{Cr}, \text{Co}, \text{Ni}$) [5, 6, 7], LiNiVO_4 [8] and $\text{Li}_2\text{FeMn}_3\text{O}_8$ [9], are of great interest and growing importance today. The viability of 5-V battery systems was recently well illustrated with the $\text{LiCr}_{0.1}\text{Ni}_{0.4}\text{Mn}_{1.5}\text{O}_4$ -based cathode, delivering an initial discharge capacity of 152 mAh/g with excellent capacity retention, at least during 30 cycles [7].

Since Padhi et al. reported in 1997 the reversible electrochemical extraction of lithium from LiFePO_4 [10], orthophosphates LiMPO_4 ($\text{M}=\text{Fe}, \text{Mn}, \text{Co}, \text{Ni}$) with olivine-like structure have received strong attention as possible candidates for lithium batteries. Among them, LiCoPO_4 was shown to reveal electrochemical lithium deinsertion–insertion at potentials close to 4.8 V vs. Li/Li^+ [11]. Initially reported by Amine et al., a discharge capacity of 70 mAh/g was extended up to 100 mAh/g by Okada et al. due to the use of another electrolyte and optimization of charge–discharge conditions [12]. Recently, Lloris et al. reported the highest discharge capacity of 125 mAh/g for this compound synthesized by a novel synthetic procedure [13]. Nevertheless, the cycling behavior was scarcely investigated in these works. Charge–discharge capacities for the first three potentiostatic and galvanostatic cycles only were given.

In our work, we discuss the electrochemical performance of LiCoPO_4 prepared by two different synthetic routes and the mechanism of lithium deinsertion–insertion for this compound.

2. Experimental:

LiCoPO₄ samples were synthesized by two different solid-state syntheses. The first one (high temperature, HT) is the direct reaction of stoichiometric amounts of Co₃O₄, Li₂CO₃ and (NH₄)₂HPO₄. The components were ground together in an agatemortar, pressed into a pellet, and calcined at 500 °C for 12 h. After additional grinding and pelletizing, the mixture was held at 800 °C for 48 h and quenched.

The alternative synthetic procedure consisted of using the cobalt-containing precursor NH₄CoPO₄ · H₂O, which was obtained as a precipitate by adding (NH₄)₂HPO₄ solution to an alkaline solution of CoCl₂ as detailed elsewhere [13]. Freshly prepared ammonium cobalt phosphate was mixed intimately with LiOH, pelletized and fired at 600 °C for 24 h. Initially, the synthesis was made in air. Modifying the synthetic conditions, we found that the sample prepared under argon flow with 20% excess of LiOH contained the lowest amount of admixtures and exhibited the best electrochemical performance. These conditions are referred to as lower-temperature (LT) synthesis.

The samples were tested by scanning electron microscopy (SEM, Philips XL-30 FEG) and X-ray powder diffraction using a STOE STADI/P powder diffractometer (MoKα₁ radiation, curved Ge(111) monochromator, transmission mode, step 0.02° (2θ), linear PSD counter). For selected samples synchrotron powder diffraction was performed at beamline B2 at the Hamburger Synchrotronstrahlungslabor HASYLAB (Germany), using the on-site readable image plate detector OBI [14] at a wavelength of 0.7095 Å. Structure characterization was performed by Rietveld analysis using the Winstep software package [15].

Electrochemical studies were carried out with a multichannel potentiation–galvanostatic system (VMP, Perkin Elmer Instruments, USA). Swagelok-type two-electrode cells were assembled in an argon-filled glove box using a lithium negative electrode and a glass-fibre separator soaked with an electrolyte solution. Aluminum and steel cylinders served as current collectors at the positive and negative sides, respectively. The electrolyte Selectin-pur-30 (Merck, Germany, 1 M LiPF₆ in EC:DMC 1:1 vol. %) was used as received. The cathode composite was fabricated as follows: 70% active material, 25% acetylene carbon black and 5% polyvinylidene fluoride as polymer binder were intimately mixed, ground in an agate mortar and pressed onto an Al mesh (resulting electrodes contain about 3 mg of active compound). For some experiments a three-electrode glass cell with different reference and counter electrodes was used. In these cases the cell was mounted and operated in a dry argon atmosphere. All experiments were performed at room temperature.

We performed our electrochemical experiments either in current-controlled or potential-controlled mode. Galvanostatic cycling was carried out at various current densities between the selected voltage limits. Electrochemical potential spectroscopy experiment (EPS) [16] conditions were set to 5-mV potential steps with $I_{lim}=0.08$ mA/cm².

3. Results and Discussion:

Characterization of the samples:

The LiCoPO₄ sample, as obtained by the HT synthesis, was found to be single-phase with an orthorhombic olivine-like structure based on XRD data. For the sample obtained under the LT synthesis conditions, orthorhombic LiCoPO₄ was identified as the main product, but additional peaks of Co₃O₄ were also detected. The amount of Co₃O₄ evaluated by Rietveld analysis was about 4%. Refined cell parameters for LiCoPO₄ (S.G. *Pmna*), prepared by different synthetic routes, are summarized in Table 1. The crystallographic data for both samples are very close to those reported for LiCoPO₄ by Amine et al. [11] and Lloris et al. [13].

Scanning electron microscopy images show significant differences in the morphology of the samples with respect to the two preparation routes (Fig. 1). Higher porosity and a smaller mean particle size are obvious for the sample obtained from the precursor NH₄CoPO₄ · H₂O. This effect can mostly be attributed to the lower synthesis temperature.

Table 1 Unit cell parameters of LiCoPO₄ synthesized by different routes

	<i>a</i> , Å	<i>b</i> , Å	<i>c</i> , Å	<i>V</i> , Å ³
HT- synthesis	10.2054(6)	5.9228(3)	4.7009(4)	284.14(3)
LT- synthesis	10.1926(8)	5.9199(5)	4.6966(4)	283.39(4)

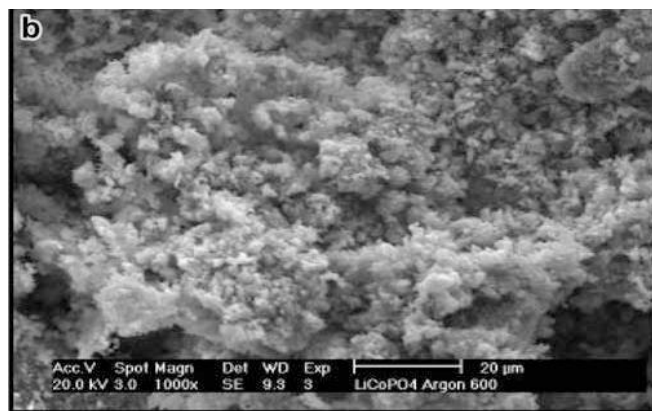
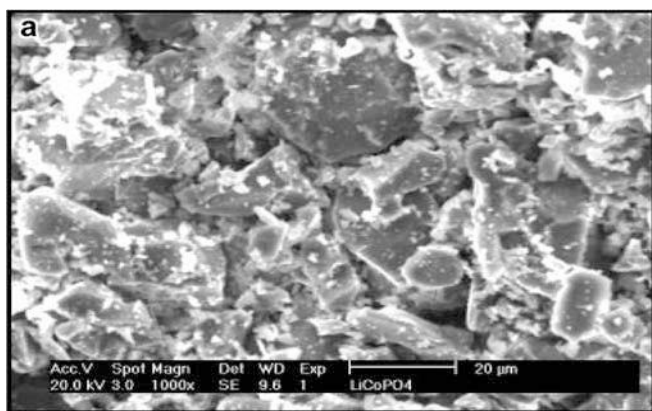


Fig. 1a,b SEM images of LiCoPO₄ samples prepared by a HT synthesis and b LT synthesis

HT-LiCoPO₄

Surprisingly, the electrochemical extraction of lithium from LiCoPO₄ prepared in HT conditions seems to be irreversible. The charge–discharge curves taken at various currents are shown in Fig. 2. In all cases plateaus close to 5 V were observed while charging the cell up to 5.1 V vs. Li/Li⁺. These plateaus do not appear any more at the following discharge, only ill-defined shoulders in the discharge profiles could be observed. The potential instability was detected at the charge plateau at low current densities (0.16 and 0.08 mA/cm²), which is probably caused by the additional electrochemical process, namely, by the decomposition of electrolyte or corrosion of current collectors. Furthermore, an appropriate discharge plateau could not be identified, even when the charging with 0.1 mA was stopped at a nearly stage with only 0.15 mol Li deinserted.

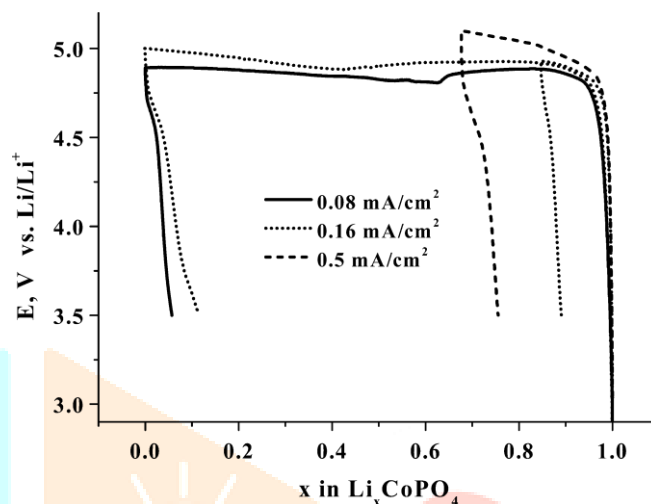


Fig. 2 First charge–discharge curves for HT-LiCoPO₄ in swagelok cell with various current densities

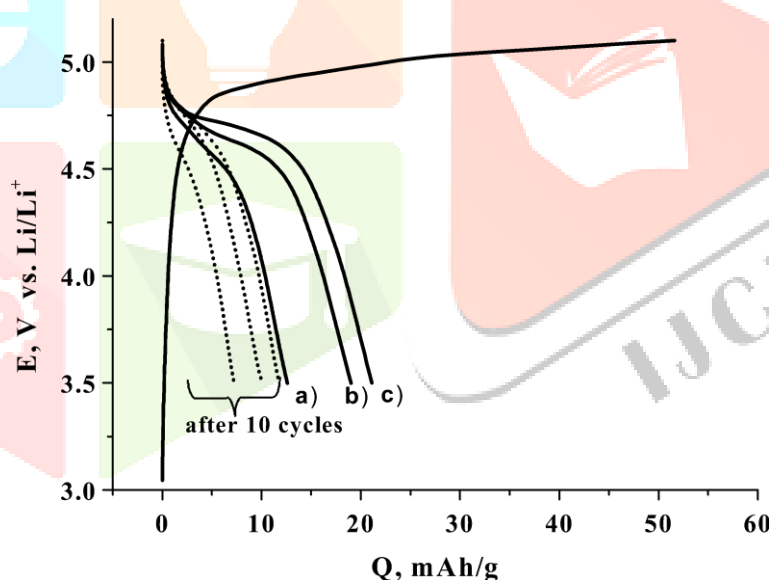


Fig. 3 Discharge curves obtained with current density a) 0.5 mA/cm², b) 0.16 mA/cm² and c) 0.08 mA/cm² after initial charging of the cell to 5.1 V with current density 0.5 mA/cm² (charge capacity 52 mAh/g)

These results are not consistent with data reported by Okada et al. [12] for LiCoPO₄ prepared under the same conditions of synthesis. After charging to 5.1 V vs. Li/Li⁺ with a rate of 0.2 mA/cm², the authors report a well-defined discharge plateau at 4.8 V with a capacity of 100 mAh/g. Furthermore, a significant decrease of the discharge capacity with increasing discharge current density was reported. In our case, the highest discharge capacity of 22 mAh/g could be achieved at a 0.08 mA/cm² discharge rate after initial charging of the cell to

5.1 V at 0.5 mA/cm² (see Fig. 3). These values are far from the capacity values reported by Okada et al. Moreover, the cells show bad cyclability, losing 50% of the initial discharge capacity after ten cycles independent of the discharge current density.

While HT-LiCoPO₄ cells reveal no reversible lithium deinsertion–insertion, it could be suggested that the charge plateaus observed in the corresponding voltage–capacity curves are most probably due to the irreversible oxidation of the electrolyte. However, ex situ XRD experiments confirm structural changes of the cathode compound during charging of the cell. The X-ray patterns of the cathode material, recorded at different stages of charging (current

density 0.16 mA/cm^2), are given in Fig. 4. With proceeding charging, a splitting of reflections is observed. This effect becomes clearer at the higher stages of charge, thereby confirming that lithium deinsertion from LiCoPO_4 really takes place. A splitting of peaks in the XRD pattern from a LiCoPO_4 electrode charged up to 5.3 V vs. Li/Li^+ was also observed by Amine et al. [11]. The authors indexed their X-ray pattern of the charged electrode based on two phases, where the unit cell volume of the first phase is close to that of the starting LiCoPO_4 , $V=283.7 \text{ \AA}^3$, while the unit cell volume of the second phase, $V=278.7 \text{ \AA}^3$, was ascribed to a lithium-poor olivine structure, $\text{Li}_{1-x}\text{CoPO}_4$.

The results of our investigation of charged LiCoPO_4 cathodes are in good agreement with those described above. A two-phase Rietveld refinement for charged $\text{Li}_{1-x}\text{CoPO}_4$ with $x=0.95$, calculated from the charge passed through the cell, was carried out. Observed, calculated and difference powder diffraction patterns are shown in Fig. 5. Initial atomic parameters for both phases were taken from the ideal LiCoPO_4 structure [17]. The first phase with the larger unit cell volume, $V=283.5(1) \text{ \AA}^3$, was considered as an ideal LiCoPO_4 structure with fully occupied lithium positions, while the second one, $V=278.4(1) \text{ \AA}^3$, was considered as an ideal CoPO_4 structure with lithium positions completely vacant (the cell parameters $a=10.037(2)$, $b=5.854(1)$, $c=4.738(1)$). The weight fractions defined from the refinement are 64(1) and 36(1)% for LiCoPO_4 and “ CoPO_4 ”, respectively. A significant deviation of the lithium-poor phase content ($x=0.95$ corresponds to 95% content of CoPO_4) calculated from the electro-chemical data may be explained by simultaneous reaction of electrolyte oxidation, which can contribute to the calculated charge. The refinement results are summarized in Table 2.

To summarize, although the two-phase mechanism of lithium extraction from the HT sample was confirmed in this investigation, there is significant discrepancy with the electrochemical data reported earlier [11, 12]. The cell parameters for LiCoPO_4 synthesized in our work and by Okada et al. are the same, but, in our opinion, the samples may have significant differences, i.e. in the real structure and particle size distribution. Unfortunately, no picture demonstrating the morphology of the samples was shown in the work of Okada and Amine, so we are unable to compare the samples properly.

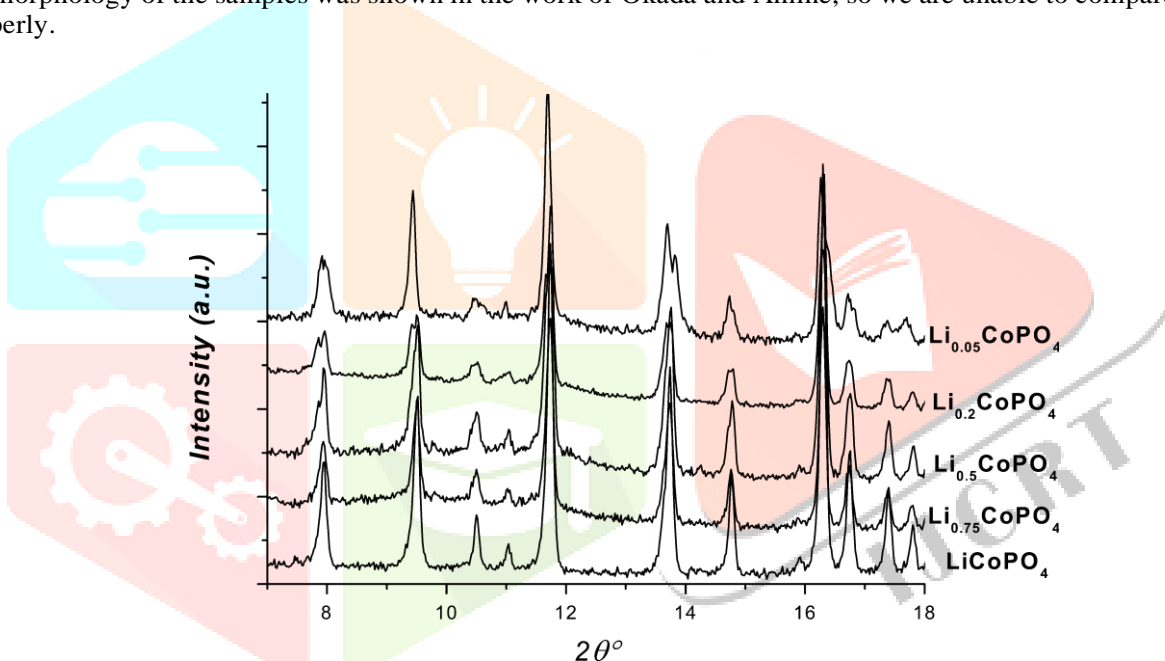


Fig. 4 X-ray powder diffraction patterns for HT- LiCoPO_4 cathode at the different stages of charging.

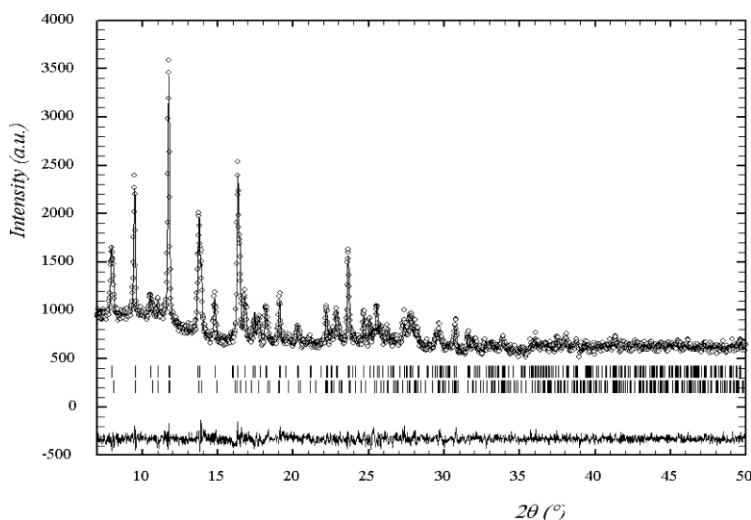


Fig. 5 Observed, calculated and difference pattern of $\text{Li}_{1-x}\text{CoPO}_4$ ($x=0.95$ calculated from the electrochemical data)

Performance of LT-LiCoPO₄

In contrast to HT-LiCoPO₄, distinct charge–discharge plateaus were observed in the voltage–capacity curves for the LiCoPO₄ sample prepared from the NH₄CoPO₄·H₂O precursor [13], see Fig. 6a. A galvanostatic experiment was also conducted at high current density (0.5 mA/cm²) to decrease the contribution from electrolyte decomposition. The charge capacity of ca. 125 mAh/g, corresponding to 75% of the theoretical value (166 mAh/g) for LiCoPO₄, was obtained at the initial charge up to 5 V vs. Li/Li⁺ in the first cycle. A discharge capacity of 92 mAh/g was achieved in the first cycle for LiCoPO₄ prepared by the low-temperature routine. Consequently, the irreversible loss of capacity detected in the first cycle comprises approximately 26%.

Atom	LiCoPO ₄			“CoPO ₄ ”			B _{eq} , Å ²
	x/a	y/b	z/c	x/a	y/b	z/c	
Li	1/2	1/2	1/2				1.0
Co	0.2787(4)	1/4	0.984(2)	0.2759(8)	1/4	0.946(2)	0.5
P	0.093(1)	1/4	0.416(2)	0.086(2)	1/4	0.381(5)	1.0
O(1)	0.100(2)	1/4	0.754(4)	0.117(3)	1/4	0.69(1)	1.0
O(2)	0.449(3)	1/4	0.213(5)	0.428(4)	1/4	0.175(7)	1.0
O(3)	0.165(2)	0.042(2)	0.284(3)	0.153(2)	0.046(4)	0.239(5)	1.0

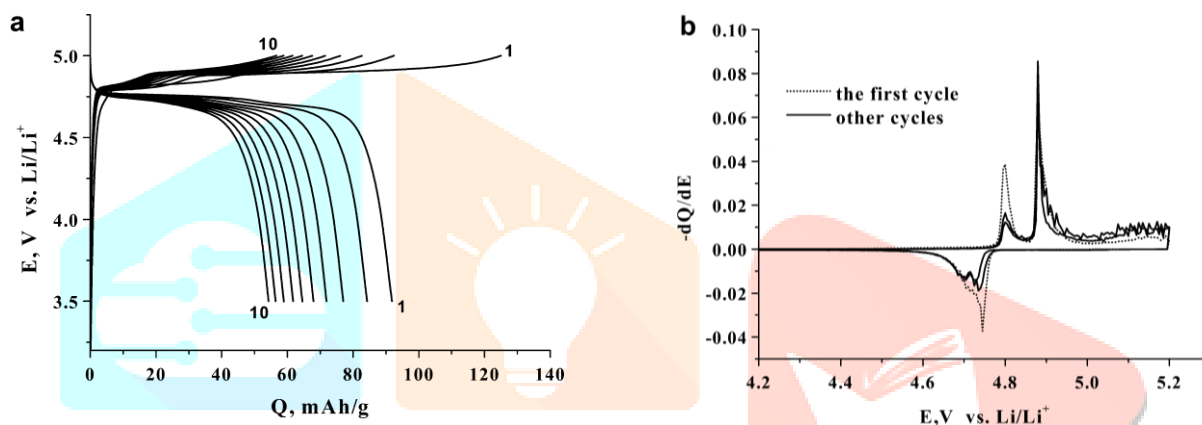


Fig. 6a,b Charge–discharge profiles of LT-LiCoPO₄ cycled between 3.5 and 5.1 V with current density 0.5 mA/cm² (a) and potentiodynamic cycling in the range 3.5–5.2 V (b)

Subsequent cycling in the voltage range 3.5–5.0 V led to severe capacity fading. Charge and discharge capacities of 57 and 54 mAh/g, respectively, were observed after ten cycles.

The characteristic feature of charging is the existence of two regions in the voltage–capacity curve, apparently indicating a two-step mechanism of lithium deinsertion. In the first cycle, the first plateau lies in the voltage range of 4.80–4.86 V, the second one is situated between 4.88 and 4.93 V vs. Li/Li⁺. At the same time, the discharge profile seems to be characteristic for a one-step mechanism. Furthermore, two peaks at 4.80 and 4.89 V at the charge of the cell were observed on the incremental capacity plot obtained on potentiodynamic cycling of the cell (see Fig. 6b). The discharge branch seems to contain two peaks too, which are badly resolved. The existence of two discharge peaks is more evident in the second and following cycles.

Figure 7 shows the first cycling curve for the LT- LiCoPO_4 cathode as a function of the charge cut-off potential, V_{charge} . Initial charging of the cell up to 4.84, 4.90 and 5.00 V vs. Li/Li^+ corresponds to an extraction of 0.2, 0.4 and 0.75 mol Li per mol LiCoPO_4 (as calculated from Faraday's law). The cycling of the cell in the narrow range of lithium contents close to the pristine LiCoPO_4 does not lead to the lower irreversible loss of capacity in the first cycle and to a better capacity retention in the following cycles, as could be expected. Consequently, the process occurring at the second plateau is not crucial for the dramatic loss of capacity and possible side reactions. Indeed, if substantial electrolyte decomposition occurs, continuous operation in the high-voltage range should result in a worse electro-chemical performance.

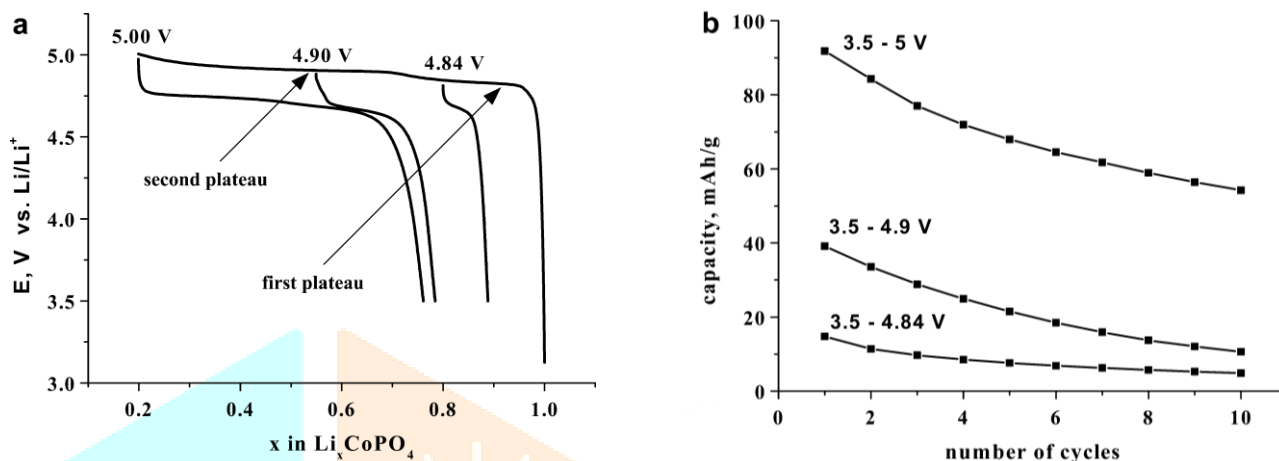


Fig. 7a,b First charge–discharge curves for LT- LiCoPO_4 , charged to the different cut-off voltages (a) and discharge capacity versus cycle number on cycling in the selected voltage ranges (b)

To eliminate the contributions due to aging of the lithium anode, galvanostatic cycling in a three-electrode setup was performed. The charge–discharge curves are shown as a capacity vs. number of cycles plot in Fig. 8. No improvement in the capacity retention was observed for three-electrode cell measurements, capacity fading is even increasing compared to the two-electrode cell setup. It indicates that processes occurring at the lithium anode during cycling the cell are not crucial for the total capacity fading. The partial restoration of capacity was observed after 20 cycles at reducing current density. Therefore, one of the reasons for the capacity loss seems to have a kinetic character, probably associated with slow lithium transport, as is known for the two-phase systems, i.e. $\text{LiFePO}_4\text{--FePO}_4$ [10]. The application of low current density does not reduce the rate of capacity fading. Evidently, the capacity loss for LiCoPO_4 has a more complicated nature. The different side reactions resulting from the electrolyte oxidation can deteriorate the reversibility of the cathode material. On the other hand, the different character of the charge and discharge curves for LT- LiCoPO_4 points to the irreversible structural transformation of the cathode compound during cycling.

To understand the origin of the two-step delithiation process from LT- LiCoPO_4 , structure investigations were performed. The $\text{Li}_{1-x}\text{CoPO}_4$ samples charged to different lithium content values, $x=0.15, 0.5$ and 0.95 (current density 0.5 mA/cm^2), were studied by ex situ synchrotron powder diffraction, see Fig. 9. Note that all these samples were measured in the same conditions, while the exposure time for the sample with $x=0$ was shorter.

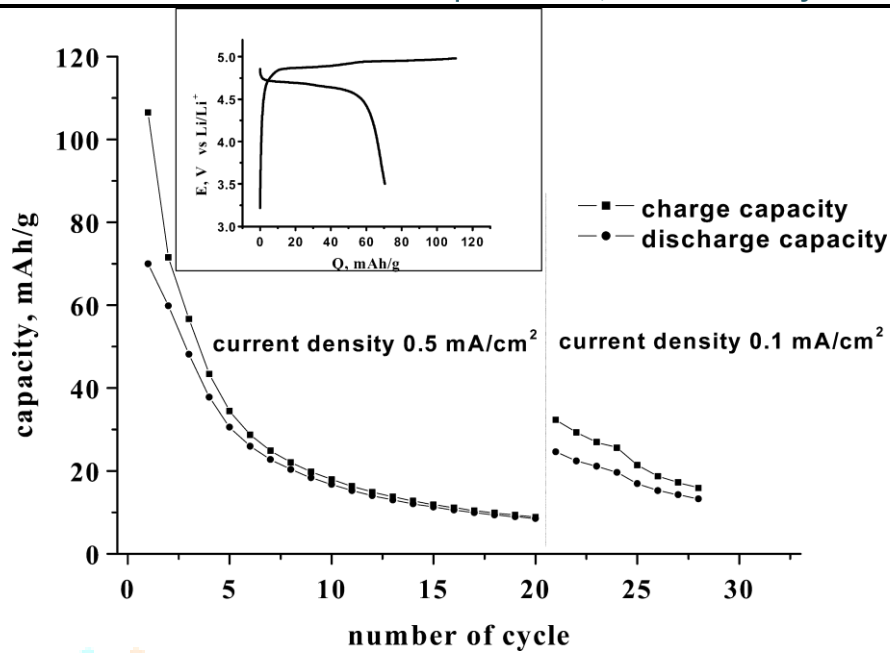


Fig. 8a,b First charge– discharge curves for LT- LiCoPO₄ cathode (a) and capacity fading during cycling the cell (b)

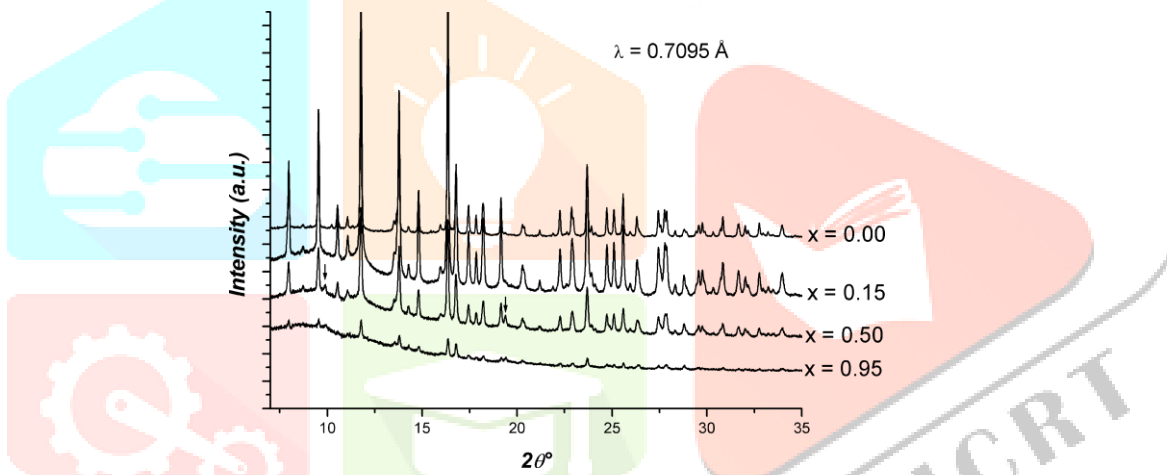


Fig. 9 Synchrotron powder diffraction pattern of LT-LiCoPO₄ cathode during charging the cell

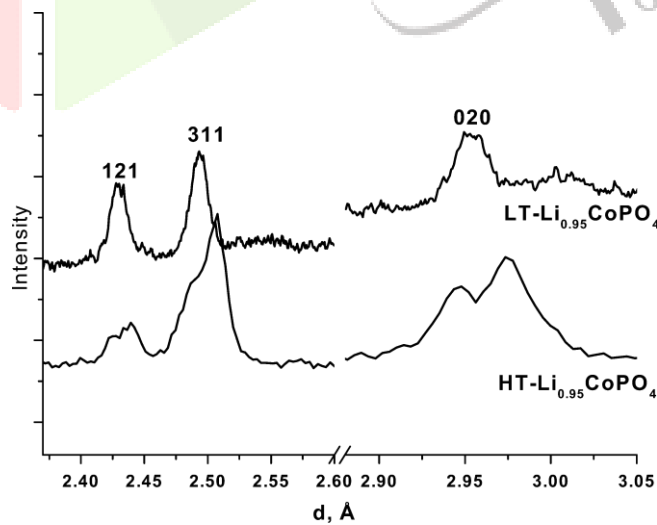


Fig. 10 Selected regions of the X-ray diffractograms for HT-LiCoPO₄ (laboratory) and LT-LiCoPO₄ samples (synchrotron) charged to x=0.95 in Li_{1-x}CoPO₄

In contrast to the HT-Li_xCoPO₄ the same values of x , neither an evident peak splitting nor changes of the cell parameters could be observed. This effect is illustrated by Fig. 10, in which two regions of the XRD diffractograms taken for samples charged to $x=0.95$ are compared. Based on the data obtained one can conclude that the charging of the LT-LiCoPO₄ cell leads to an amorphization of the cathode material, which was found to be less at low current densities. Furthermore, some broad peaks of the unknown phase appear at the deep stages of charging; these peaks are marked by arrows in Fig. 9. Consequently, the first delithiation of LT-LiCoPO₄ proceeds via a mechanism which differs drastically from the one established for HT-LiCoPO₄.

4. Conclusions:

A strong dependence of the electrochemical performance of LiCoPO₄ cathodes on the different synthetic routes was established. The electrochemical behaviour of the HT-LiCoPO₄ we prepared differs significantly from the literature data for the sample obtained under similar synthetic conditions. Based on the galvanostatic cycling data and X-ray powder diffraction studies we could establish irreversible delithiation of this sample, proceeding through the formation of a crystalline lithium-poor phase. In contrast to HT-LiCoPO₄, the low-temperature synthesis leads to a significant improvement of the electrochemical performance, which might be correlated to the smaller mean particle size of the sample, as well as to the different mechanisms of delithiation observed. The main characteristic feature of the delithiation process of LT-LiCoPO₄ is the two-step plateau in the voltage–capacity curve. At the same time, lithium deinsertion of LT-LiCoPO₄ does not lead to the formation of a lithium-poor phase as in the case of HT-LiCoPO₄ and LiFePO₄.

Despite of the reversible delithiation of LT-LiCoPO₄, capacity fade during cycling is still very high. The irreversible structural transformations seem to occur during charging, resulting in the fast deterioration of electrochemical performance. Amorphization of the samples during the first charge as well as the presence of an unknown phase are supported by the XRD data. Further investigations to understand the structural changes occurring during charge–discharge cycles are in progress.

5. References:

- Mizushima K, Jones PC, Wiseman PJ, Goodenough JB (1980) *Mat Res Bull* 15:783
- Reimers JN, Dahn JR (1992) *J Electrochem Soc* 139:2091
- Tarascon JM, Guyomard D (1993) *Electrochim Acta* 38:1221
- Caurant D, Baffier N, Garsia, B, Pereira-Ramos JP (1996) *Solid State Ionics* 91:45
- Sigala C, Guyomard D, Verbaere A, Piffard Y, Tournoux M (1995) *Solid State Ionics* 81:167
- Alcañtara R, Jaraba M, Lavela P, Tirado JL (2002) *Electrochim Acta* 47:1829
- Hong KJ, Sun YK (2002) *J Power Sources* 109:427
- Fey GT-K, Li W, Dahn JR (1994) *J Electrochem Soc* 141:2279
- Kawai H, Nagata M, Tabuchi M, Tukamoto H, West AR (1998) *Chem Mater* 10:3266
- Padhi AK, Nanjundaswamy KS, Goodenough JB (1997) *J Electrochem Soc* 144:1188
- Amine K, Yazuda H, Yamachi M (2000) *Electrochem Solid-State Lett* 3:178
- Okada S, Sawa S, Egashira M, Yamaki J, Tabuchi M, Kageyama H, Konishi T, Yoshino A J (2001) *J Power Sources* 97–98:430
- Lloris JM, Peñez Vicente C, Tirado JL (2002) *Electrochem Solid-State Lett* 5:A234-A237
- Knapp M, Joco V, Baetz C, Brecht HH, Berghaeuser A, Ehrenberg H, von Seggern H, Fuess H (2003) *Nucl Instrum Methods* (submitted)
- Roisnel T, Rodriguez-Carvajal J (2002), WinPLOTR: a graphical tool for powder diffraction
- Thompson AH (1979) *J Electrochem Soc* 126:608
- Kubel F (1994) *Z Kristallgr* 209:755